Eur. Phys. J. C 9, 413–424 (1999)
Digital Object Identifier (DOI) 10.1007/s100529900032

THE EUROPEAN PHYSICAL JOURNAL C

Higgs production: CP studies in e^-e^- collisions

C. A. Bøe[1], O. M. Ogreid[1], P. Osland[1], Jian-zu Zhang[2]

[1] Department of Physics, University of Bergen, Allégaten 55, N-5007 Bergen, Norway
[2] School of Science, East China University of Science and Technology, 130 Mei Long Road, Shanghai 200237, P. R. China

Received: 1 December 1998 / Revised version: 15 February 1999 / Published online: 18 June 1999

Abstract. We review the production of scalar Higgs-like particles in high-energy electron–electron collisions, via the fusion of electroweak gauge bosons. The emphasis is on how to distinguish a CP-even from a CP-odd Higgs particle. Among the more significant differences, we find that in the CP-odd case, the Higgs spectrum is much harder, and the dependence of the total cross section on the product of the polarizations of the two beams much stronger, than in the CP-even case. We also briefly discuss parity violation, and the production of charged Higgs bosons.

1 Introduction

In planning for a future linear collider [1,2] one has to explore not only the electron–positron mode and various photon modes, but also an electron–electron mode, in spite of concerns related to beam "disruption". One reason that an electron–electron collider is interesting is that one may produce states not accessible in the annihilation channel; another is that a large electron polarization will be readily available. There is already a considerable literature on the electron–electron mode [3–6].

We consider here the production of Higgs particles[1] in electron–electron collisions. Apart from a precise determination of the Higgs mass, which will allow for certain consistency tests of the theory, one would want to determine its properties under the discrete symmetries, and its couplings to various other particles. At high energies, the Higgs production at an electron–electron collider will proceed via gauge boson fusion [3,6], and thus not be suppressed by the s-channel annihilation mechanism [7]. Certain models also predict doubly-charged Higgs particles [8], some of which can be produced more readily at an electron–electron collider.

Scalar ("Higgs") particles, h, h^- and h^{--}, are produced in the t-channel via Z- or W-exchange:

$$e^-(p_1) + e^-(p_2) \to e^-(p_1') + e^-(p_2') + h(p_h), \quad (1.1)$$
$$e^-(p_1) + e^-(p_2) \to e^-(p_1') + \nu_e(p_2') + h^-(p_h), \quad (1.2)$$
$$e^-(p_1) + e^-(p_2) \to \nu_e(p_1') + \nu_e(p_2') + h^{--}(p_h), \quad (1.3)$$

as depicted in Fig. 1 for the case (1.1). (However, in some models, including the left–right symmetric model [9], the doubly-charged Higgs boson has practically no coupling to the ordinary, left-handed W bosons. They would not be produced by this mechanism.) It is well known that the CP property of the Higgs particle can be explored in the electron–positron annihilation mode from studies of angular and energy correlations [10–12]. In the present paper, we analyze the corresponding situation for the t-channel, at an electron–electron collider, taking into account the effects of beam polarization. We shall investigate to what extent various angular distributions and energy correlations are sensitive to whether the Higgs particle is even or odd under CP, in which case it will be denoted as H or A, respectively. It turns out that several of these distributions are quite sensitive to the CP property of the Higgs particle. Some of these results were presented elsewhere [13]. The ZZh coupling is taken to be [14]

$$\mathrm{i}2^{5/4}\sqrt{G_F}\begin{cases} m_Z^2\, g^{\mu\nu} & \text{for } h = H \ (CP \text{ even}), \\ \eta\, \epsilon^{\mu\nu\rho\sigma} k_{1\rho} k_{2\sigma} & \text{for } h = A \ (CP \text{ odd}), \end{cases} \quad (1.4)$$

where k_1 and k_2 are the momenta of the gauge bosons. Thus, we see immediately that near the forward direc-

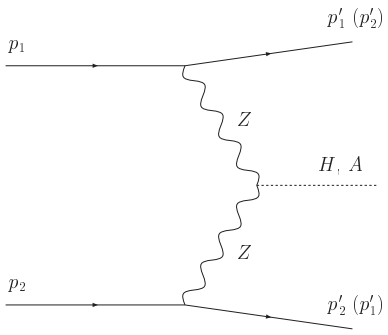

Fig. 1. Feynman diagram for the class of processes considered. (There is also a crossed diagram.)

[1] The term "Higgs particle" will here be used quite generally about any scalar, electrically neutral or charged, that has a significant coupling to electroweak gauge bosons.

tion, where $\boldsymbol{k}_1$ and $\boldsymbol{k}_2$ are antiparallel, the production of a CP-odd Higgs boson will be suppressed. In the MSSM, this ZZA coupling is absent at the tree level, but will be induced at the 1-loop level [15], with a strength $\eta = \mathcal{O}(\alpha)$ multiplied by a complicated function of the masses involved. Our analysis is not restricted to any particular model.

There could also be CP violation in the Higgs sector, in which case the Higgs bosons would not be CP eigenstates [16]. Such mixing could take place at the tree level [17], or it could be induced by radiative corrections. It has also been pointed out that such mixing might take place in the MSSM, and be resonant [18]. We shall discuss ways to look for CP violation in the effective ZZh coupling.

The focus will be on a light Higgs boson, as is favored by current LEP precision data [19], and the case of $E_{\mathrm{c.m.}} = 500$ GeV [2]. When one or both Zs are replaced by Ws (for the production of charged Higgs particles), we shall assume that the Lorentz structure of the coupling remains unchanged. The paper is organized as follows. In Sect. 2 we give notations and discuss kinematics. In Sect. 3 we give various cross section formulas. In Sects. 4–6 we present a variety of numerical results. Section 4 is devoted to integrated cross sections and distributions where the final-state electrons are integrated over. These distributions would qualitatively be the same for the production of charged Higgs particles. In Sect. 5 we study correlations between the final-state electrons, and in Sect. 6 we consider parity violation. Sect. 7 is devoted to a brief qualitative discussion of charged Higgs particles. In Sect. 8 we discuss statistics, and in Sect. 9. give some concluding remarks.

2 Notation and kinematics

The eeZ vector and axial vector couplings are denoted g_V and g_A, as defined by the interaction $\overline{\psi}(x)\gamma^\mu(g_V - g_A\gamma_5)\psi(x)Z_\mu(x)$. As a parameterization of their ratio, we define the angle χ by

$$g_V \equiv \tilde{g}\cos\chi, \qquad g_A \equiv \tilde{g}\sin\chi, \tag{2.1}$$

with

$$\tilde{g}^2 = \left(\frac{g}{4\cos\theta_{\mathrm{W}}}\right)^2 [(1-4\sin^2\theta_{\mathrm{W}})^2 + 1], \tag{2.2}$$

and g the SU(2) electroweak coupling constant. In the present work, the only reference to this angle χ is through $\sin 2\chi$. In the case of the eeZ coupling, we have $\sin 2\chi \simeq 0.1393$, whereas for the $e\nu W$ coupling, which is purely left-handed, we have $\sin 2\chi = 1$. This overall constant is of the order of $\tilde{g}^2 \sim 4\pi\alpha/3$.

The momenta of the final-state leptons will be referred to by polar angles θ_1 and θ_2 (see (1.1)), and that of the Higgs particle by the polar angle θ_h:

$$\begin{aligned}
\boldsymbol{p}_1\cdot\boldsymbol{p}_1' &= |\boldsymbol{p}_1||\boldsymbol{p}_1'|\cos\theta_1 = EE_1'\cos\theta_1,\\
\boldsymbol{p}_1\cdot\boldsymbol{p}_2' &= |\boldsymbol{p}_1||\boldsymbol{p}_2'|\cos\theta_2 = EE_2'\cos\theta_2,\\
\boldsymbol{p}_1\cdot\boldsymbol{p}_h &= |\boldsymbol{p}_1||\boldsymbol{p}_h|\cos\theta_h = E\sqrt{E_h^2 - m_h^2}\cos\theta_h.
\end{aligned} \tag{2.3}$$

For forward production, we will thus have $\cos\theta_1 \simeq 1$, $\cos\theta_2 \simeq -1$. Furthermore, an azimuthal angle ϕ will refer to the relative orientation of the two planes formed by the final and initial-state leptons (in [13] the definition used was $\cos\phi \to -\cos\phi$),

$$\cos\phi = \frac{(\boldsymbol{p}_1\times\boldsymbol{p}_1')\cdot(\boldsymbol{p}_1\times\boldsymbol{p}_2')}{|\boldsymbol{p}_1\times\boldsymbol{p}_1'||\boldsymbol{p}_1\times\boldsymbol{p}_2'|}\,. \tag{2.4}$$

The two beams will be taken to be longitudinally polarized, with degrees of polarizations given by P_1 and P_2, respectively ($P_i > 0$ for a right-handed polarization). We shall express the cross sections in terms of the variables

$$\begin{aligned}
s_1 &= (p_1+p_2)^2, & s_2 &= (p_1'+p_2')^2,\\
t_1 &= (p_1-p_1')^2, & t_2 &= (p_2-p_2')^2,\\
u_1 &= (p_1-p_2')^2, & u_2 &= (p_2-p_1')^2,
\end{aligned} \tag{2.5}$$

where (neglecting the electron mass)

$$m_h^2 = s_1+s_2+t_1+t_2+u_1+u_2. \tag{2.6}$$

For the two final-state electrons, we distinguish p_1' and p_2', according to which has the higher energy, $E_1' > E_2'$.

3 The $e^-e^- \to h\,e^-e^-$ cross section

For Higgs production from an electron–electron initial state via the so-called fusion mechanism (with Z exchange), there are two diagrams, because of the symmetry of the two electrons in the final state. The corresponding two amplitudes differ by the substitutions $p_1' \leftrightarrow p_2'$, corresponding to $(t_1,t_2) \leftrightarrow (u_1,u_2)$, and by an overall sign.

We present the differential cross section in two different forms. Both are useful, according to which distribution we want to study. For the study of distributions of the final-state electrons, we express the differential cross section as

$$\begin{aligned}
\frac{\mathrm{d}^4\sigma^{(h)}}{\mathrm{d}\varepsilon\,\mathrm{d}\cos\theta_1\,\mathrm{d}\cos\theta_2\,\mathrm{d}\phi} &= C^{(h)}\big\{|F(t_1,t_2)|^2\,X^{(h)}\\
&\quad + (t_j \leftrightarrow u_j) + 2\mathrm{Re}[F^*(u_1,u_2)F(t_1,t_2)]Z^{(h)}\big\},
\end{aligned} \tag{3.1}$$

where $F(t_1,t_2)$ is a propagator factor,

$$F(t_1,t_2) = \frac{1}{t_1-m_Z^2}\,\frac{1}{t_2-m_Z^2}. \tag{3.2}$$

The overall constant is given as[2]

$$C^{(h)} = \frac{1}{(2\pi)^4}\frac{G_{\mathrm{F}}}{\sqrt{2}}\frac{\tilde{g}^4}{2s}\frac{m_Z^4E_1'E_2'}{|J|E_h}\begin{cases}1 & \text{for } h=H,\\ \eta^2 & \text{for } h=A,\end{cases} \tag{3.3}$$

[2] The normalizations of $C^{(h)}$ and ε take into account the fact that there are two identical particles in the final state. Since the two electrons are distinguished by their energies, the polar angles θ_1 and θ_2 may take on any values in the range $[0,\pi]$.

with the Jacobian

$$J = 1 + \frac{2E - E_h}{2E_h}(1 + \hat{\boldsymbol{p}}_1' \cdot \hat{\boldsymbol{p}}_2'), \tag{3.4}$$

and ε half the energy difference between the two electrons,

$$\varepsilon = \tfrac{1}{2}(E_1' - E_2'). \tag{3.5}$$

Since the two final-state electrons are indistinguishable, we shall identify the momenta such that $E_1' \geq E_2'$; thus, $\varepsilon \geq 0$. The maximum value is given by the beam energy and the Higgs mass as

$$\varepsilon_{\max} = \frac{1}{2}E - \frac{m_h^2}{8E}. \tag{3.6}$$

For the purpose of studying distributions in $\cos\theta_h$ and E_h, it is more convenient to express the cross section as[3]

$$\frac{\mathrm{d}^4\sigma^{(h)}}{\mathrm{d}E_h\,\mathrm{d}\cos\theta_1\,\mathrm{d}\cos\theta_h\,\mathrm{d}\phi_h} = \tilde{C}^{(h)}\big\{|F(t_1,t_2)|^2\,X^{(h)} + (t_j \leftrightarrow u_j) + 2\mathrm{Re}[F^*(u_1,u_2)F(t_1,t_2)]Z^{(h)}\big\}, \tag{3.7}$$

where the overall constant is given as

$$\tilde{C}^{(h)} = \frac{1}{(2\pi)^4}\frac{G_\mathrm{F}}{\sqrt{2}}\frac{\tilde{g}^4}{2s}\frac{m_Z^4 E_1'\sqrt{E_h^2 - m_h^2}}{|\tilde{J}|E_2'}\begin{cases}1 & \text{for } h = H,\\ \eta^2 & \text{for } h = A,\end{cases} \tag{3.8}$$

and $\tilde{J}$ is the Jacobian,

$$\tilde{J} = 1 + \frac{1}{E_2'}\left(E_1' + (\hat{\boldsymbol{p}}_1' \cdot \hat{\boldsymbol{p}}_h)\sqrt{E_h^2 - m_h^2}\right). \tag{3.9}$$

The dynamics is given by $X^{(h)}$ and $Z^{(h)}$. Below, we consider three cases: (1) The CP-even case, (2) the CP-odd case, and (3) the case of CP violation.

3.1 The CP-even case

For the CP-even case, we find

$$\begin{aligned} X^{(H)} &= 2\big[(1 - P_1\sin 2\chi)(1 - P_2\sin 2\chi)(s_1s_2 + u_1u_2) \\ &\quad + (\sin 2\chi - P_1)(\sin 2\chi - P_2)(s_1s_2 - u_1u_2)\big], \\ Z^{(H)} &= 2\big[(1 - P_1\sin 2\chi)(1 - P_2\sin 2\chi) \\ &\quad + (\sin 2\chi - P_1)(\sin 2\chi - P_2)\big]s_1s_2. \end{aligned} \tag{3.10}$$

[3] When integrating over (3.7) to obtain less-differential cross sections, one has to keep in mind that there are two identical electrons in the final state, and integrate $\cos\theta_1$ over only one hemisphere.

3.2 The CP-odd case

For the CP-odd case, we find

$$\begin{aligned} X^{(A)} &= (1 - P_1\sin 2\chi)(1 - P_2\sin 2\chi)Y_0 \\ &\quad + (\sin 2\chi - P_1)(\sin 2\chi - P_2)Y_2, \\ Z^{(A)} &= \big[(1 - P_1\sin 2\chi)(1 - P_2\sin 2\chi) \\ &\quad + (\sin 2\chi - P_1)(\sin 2\chi - P_2)\big]Y, \end{aligned} \tag{3.11}$$

with

$$\begin{aligned} Y_0 &= \frac{1}{2m_Z^4}\big\{t_1t_2[(s_1 + s_2)^2 + (u_1 + u_2)^2] \\ &\quad - 2[(s_1s_2 - u_1u_2)^2 + (t_1t_2)^2]\big\}, \\ Y_2 &= \frac{1}{2m_Z^4}t_1t_2[(s_1 - s_2)^2 - (u_1 - u_2)^2], \end{aligned} \tag{3.12}$$

and

$$\begin{aligned} Y &= \frac{1}{4m_Z^4}[s_1s_2(s_1^2 + s_2^2) - (s_1 + s_2)^2(t_1t_2 + u_1u_2) \\ &\quad + 2(t_1t_2 - u_1u_2)^2]. \end{aligned} \tag{3.13}$$

For comparison, we give in Appendix A the corresponding results, including beam polarization effects, as well as the t-channel contribution, for the more familiar case of

$$e^+(p_1) + e^-(p_2) \to e^+(p_1') + e^-(p_2') + h(p_h). \tag{3.14}$$

3.3 CP violation

To allow for the possibility of CP violation in the interaction between electroweak gauge bosons and the Higgs, we introduce a mixing angle α as follows:

$$\mathcal{M} = \cos\alpha\,\mathcal{M}_\mathrm{even} + \sin\alpha\,\mathcal{M}_\mathrm{odd}. \tag{3.15}$$

Thus, for $\alpha = 0$ or $\pi/2$, the Higgs has even or odd CP, respectively, whereas for $\sin 2\alpha \neq 0$, the production mechanism violates CP. This amounts to allowing for both terms, and their interference. The suitably averaged square of the amplitude will then take the form

$$\begin{aligned} \sum_\mathrm{spin}|\mathcal{M}|^2 &= \cos^2\alpha\sum_\mathrm{spin}|\mathcal{M}_\mathrm{even}|^2 + \sin^2\alpha\sum_\mathrm{spin}|\mathcal{M}_\mathrm{odd}|^2 \\ &\quad + \sin 2\alpha\,\mathrm{Re}\sum_\mathrm{spin}\mathcal{M}_\mathrm{even}^\dagger\mathcal{M}_\mathrm{odd}. \end{aligned} \tag{3.16}$$

In the notation of (3.1) and (3.7), we get

$$\begin{aligned} X^{(h)} &= \cos^2\alpha\,X^{(H)} + \sin^2\alpha\,X^{(A)} + \sin 2\alpha\,\tilde{X}, \\ Z^{(h)} &= \cos^2\alpha\,Z^{(H)} + \sin^2\alpha\,Z^{(A)}, \end{aligned} \tag{3.17}$$

where the amount of CP violation is given by $\sin 2\alpha$, with

$$\tan\alpha = \eta, \tag{3.18}$$

as follows from an identification of (3.15) with (1.4). The CP-even terms $X^{(H)}$ and $Z^{(H)}$ are given by (3.10), and the CP-odd ones, $X^{(A)}$ and $Z^{(A)}$, by (3.11)–(3.13). There is no CP-violating contribution to the interference between the t- and u-channel terms. For the t- and u-channel CP-violating terms, which are proportional to

$$H \equiv \frac{1}{m_Z^2}\,\epsilon_{\mu\nu\rho\sigma} p_1^\mu p_2^\nu p_1'^\rho p_2'^\sigma = -2(E/m_Z)^2\,\hat{\boldsymbol{p}}_1 \cdot (\boldsymbol{p}_1' \times \boldsymbol{p}_2'), \tag{3.19}$$

we find

$$\begin{aligned}\tilde{X}_t &= 2\{[(1+P_1P_2)(1+\sin^2 2\chi) - 2(P_1+P_2)\sin 2\chi] \\ &\quad \times(s_1+s_2) - (1-P_1P_2)(1-\sin^2 2\chi)(u_1+u_2)\}H, \\ \tilde{X}_u &= -2\{[(1+P_1P_2)(1+\sin^2 2\chi) - 2(P_1+P_2)\sin 2\chi] \\ &\quad \times(s_1+s_2) - (1-P_1P_2)(1-\sin^2 2\chi)(t_1+t_2)\}H.\end{aligned} \tag{3.20}$$

A quantitative study of this case of CP violation is presented in Sect. 6.

4 Gross features of the cross section

The Z propagators will favor production at small momentum transfers, i.e., with the final-state electrons close to the beam directions. This is indeed how the CP-even Higgs particle is produced. However, a finite momentum transfer is required to produce a CP-odd particle, as is seen from the coupling (1.4) and also from the explicit expressions (3.11)–(3.13). This statement will be illustrated quantitatively below.

4.1 Total cross section

For a collider at $\sqrt{s} = 500$ GeV, the cross section for producing a Standard Model Higgs with a mass of 100 GeV is 9 fb, and falls steeply with mass, as illustrated in Fig. 2 (denoted "even"). The corresponding Bjorken cross section is around 60 fb [2]. We also compare with the cross section for producing a CP-odd Higgs boson, taking the coupling strength η such that the two cross sections coincide at $m_h = 100$ GeV[4].

Since it may be difficult to observe electrons at small angles, and in order to reduce certain backgrounds, we also study the effect of a cut, with respect to the beam, on the polar angles of the final-state electrons. Three sets of curves are given in Fig. 2. The upper ones are for no cut, whereas the lower ones correspond to cuts at 5° (as suggested by Minkowski [6]) and at 15°[5]. Similar results are given by Hikasa [3] at higher energies[6], and in [6].

[4] Clearly, in this phenomenological coupling, (1.4), the strength η might depend on the Higgs mass.

[5] This more conservative cut was studied by Barger et al. [6]

[6] Our cross section agrees with Fig. 6 of [3].

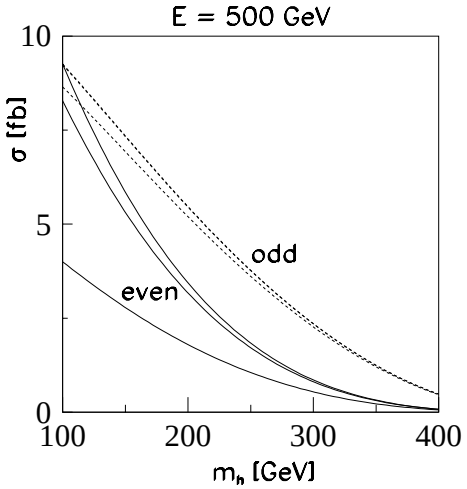

Fig. 2. Cross sections for Higgs production in electron–electron collisions at $E_{\mathrm{c.m.}} = 500$ GeV, for a range of Higgs masses. Standard Model (denoted "even") and CP-odd results are shown. For each case, the upper curve corresponds to no cut, whereas the middle and lower ones are obtained with angular cuts at 5° and 15°, respectively. (In the odd case, the curve for 5° cannot be distinguished from the one for no cut.) The cross sections for the odd case are normalized such that for no cuts, they coincide at $m_h = 100$ GeV, yielding $\eta = 0.884$ (see (1.4))

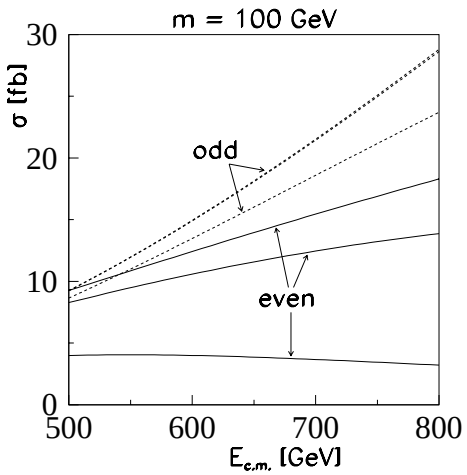

Fig. 3. Cross sections for Higgs production in electron–electron collisions for a Higgs mass $m_h = 100$ GeV, for a range of energies, $E_{\mathrm{c.m.}}$. Standard Model (denoted "even") and CP-odd results are shown. For each case, the upper curve corresponds to no cut, whereas the lower ones are obtained with the same angular cuts as those in Fig. 2. The cross sections for the odd case are normalized as in Fig. 2

The energy dependence is illustrated in Fig. 3. As the energy increases, the cross section grows. This is characteristic of the t-channel fusion mechanism, and rather different from the case of the Bjorken mechanism. However, an angular cut will temper this growth with energy; for the CP-even case, the cross section may even decrease with energy (see also [6]). Polarization-dependent total cross sections will be discussed in Sect. 4.4.

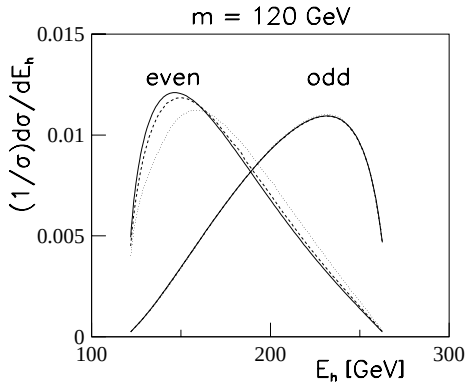

a

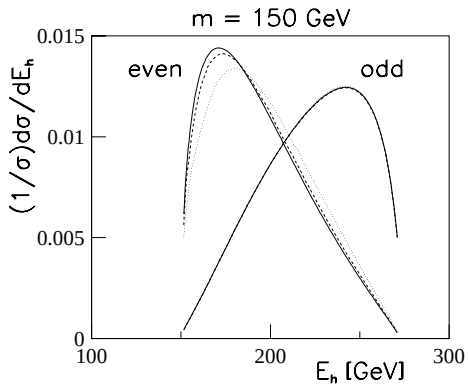

b

Fig. 4a,b. Higgs energy spectra for the case $E_{\mathrm{c.m.}} = 500$ GeV, and for Higgs masses $m_h = 120$ GeV and 150 GeV. The solid curves give the distributions in the absence of any cut. The dashed and dotted curves show the corresponding distributions when cuts at 5° and 10° are imposed on the electron momenta

4.2 Higgs energy distributions

It is interesting to consider the Higgs energy distribution

$$\frac{1}{\sigma^{(h)}}\frac{\mathrm{d}\sigma^{(h)}}{\mathrm{d}E_h} = \frac{1}{\sigma^{(h)}}\int_0^1 \mathrm{d}\cos\theta_1 \int_{-1}^1 \mathrm{d}\cos\theta_h \int_0^{2\pi} \mathrm{d}\phi \times \frac{\mathrm{d}^4\sigma^{(h)}}{\mathrm{d}E_h\,\mathrm{d}\cos\theta_1\,\mathrm{d}\cos\theta_h\,\mathrm{d}\phi}\,. \quad (4.1)$$

We show such distributions in Fig. 4, for $\sqrt{s} = 500$ GeV, and for two Higgs masses, $m_h = 120$ GeV and 150 GeV. In the CP-even case, the Higgs particle has rather low energy, whereas in the CP-odd case, the spectrum is much harder, as discussed previously.

When one imposes a cut on the opening angle of the final-state electron momenta with respect to the beam, the CP-even spectrum becomes harder, whereas the CP-odd one is practically unchanged. Curves are shown (dashed and dotted) in Fig. 4, corresponding to cuts at opening angles of 5 and 10 degrees. (No cut is imposed on the Higgs particle.) However, even with such a cut, there is a clear distinction between the two cases. We shall return to these distributions in Sect. 8.

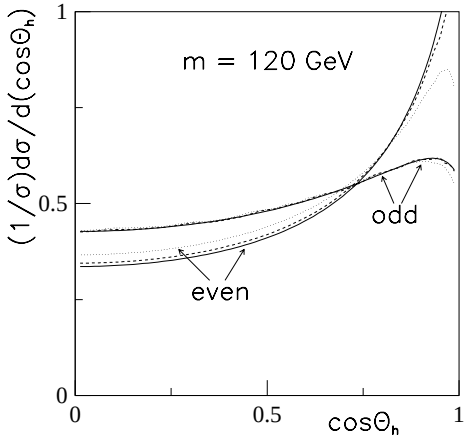

a

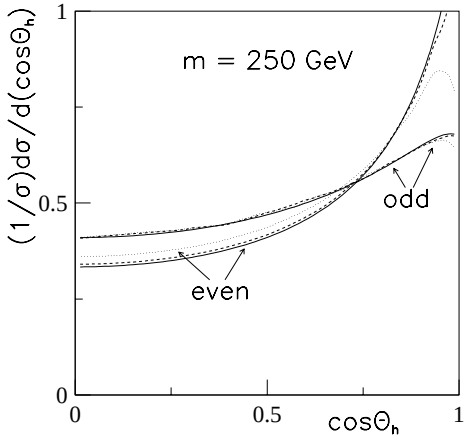

b

Fig. 5a,b. Distributions in $\cos\theta_h$, for $E_{\mathrm{c.m.}} = 500$ GeV and two mass values: $m_h = 120$ GeV and 250 GeV. Both the CP-even and the CP-odd cases are considered, as indicated. Solid curves correspond to no cuts, and dashed and dotted curves correspond to cuts on the final-state electrons at 5° and 10°, respectively

4.3 Higgs polar-angle distributions

Next, we consider the Higgs polar-angle distribution

$$\frac{1}{\sigma^{(h)}}\frac{\mathrm{d}\sigma^{(h)}}{\mathrm{d}\cos\theta_h} = \frac{1}{\sigma^{(h)}}\int_0^1 \mathrm{d}\cos\theta_1 \int_0^{2\pi} \mathrm{d}\phi \times \int_{m_h}^{E_{h\,\max}} \mathrm{d}E_h \frac{\mathrm{d}^4\sigma^{(h)}}{\mathrm{d}E_h\,\mathrm{d}\cos\theta_1\,\mathrm{d}\cos\theta_h\,\mathrm{d}\phi}\,. \quad (4.2)$$

The range of integration over E_h is determined by $m_h \le E_h \le E + m_h^2/(4E)$. In Fig. 5 we show such distributions for $\sqrt{s} = 500$ GeV and for two values of the Higgs mass: $m_h = 120$ GeV and 250 GeV.

In the absence of any cut, there is a clear distinction between the two cases of CP, the CP-even distribution being much more peaked along the beam direction. When cuts are imposed on the opening angles of the final-state electrons, this difference is reduced, but not seriously. The dashed and dotted curves in Fig. 5 show the effects of imposing a cut on the opening angle of the final-state elec-

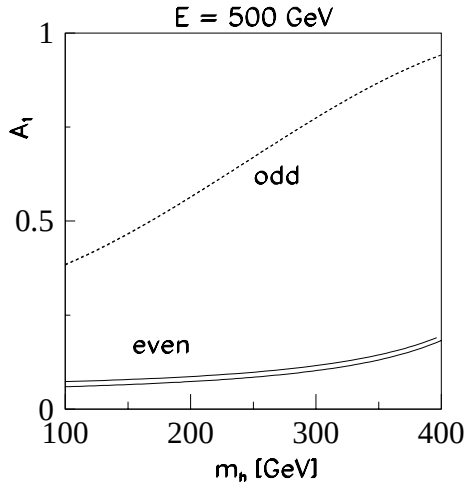

Fig. 6. The bi-polarization-dependence A_1 (see (4.3)) as obtained from the integrated cross sections for Higgs production in electron–electron collisions at $E_{\mathrm{c.m.}} = 500$ GeV, for a range of Higgs masses. Standard Model (denoted "even") and CP-odd results are shown. For the even case, the lower curve corresponds to no cut; the upper curves are obtained with an angular cut on the final-state electron momenta at 10°. (For the odd case, the two curves are indistinguishable)

trons, with respect to the beam, of 5 and 10 degrees, respectively. The dependence of these distributions on the Higgs mass, is very weak. Such polar-angle distributions may therefore be valuable, in particular if one can get data near the beam directions.

4.4 Polarization-dependent correlations

The dependence on longitudinal beam polarization is given by

$$\mathrm{d}^4\sigma^{(h)} = \mathrm{d}^4\sigma_0^{(h)}\left[1 + A_1^{(h)}\,P_1P_2 + A_2^{(h)}(P_1+P_2)\right] \quad (4.3)$$

where $|A_1^{(h)}| \le 1$, and $|A_2^{(h)}| \le \frac{1}{2}(1+A_1^{(h)})$ [20]. The quantities $A_1^{(h)}$ and $A_2^{(h)}$ might be useful in distinguishing the even and odd case, since the unknown coupling strength η cancels out.

The quantity A_1 is most easily extracted if both beams have equal and opposite polarizations. A_1 is shown in Fig. 6 for the integrated cross section. There are very strong differences between the two CP cases. For the CP-odd case, the cross section is much reduced if the two beams have large and opposite polarizations, whereas in the even case, there is only a small reduction. The large value of A_1 in the CP-odd case implies that the cross section is greatly reduced if both beams are longitudinally polarized. This suppression is due to the fact that in the CP-odd case, the two intermediate Zs must have orthogonal polarizations[7]. In the extraction of A_1 from data, there will be a contamination from the A_2 term in (4.3) when $P_1 + P_2 \neq 0$. For the parameters given in Fig. 6, A_2 ranges from -16% to -18% and from -21% to -30% for the CP-even and -odd cases, respectively.

[7] We are grateful to P. Zerwas for this observation.

5 Final-state electron–electron correlations

In the electron–electron mode, the angular distributions are more complicated than in the positron–electron mode, because the propagators depend on the angles of interest, through t_j and u_j.

5.1 Azimuthal correlations

We first consider distributions in the azimuthal angle ϕ defined in (2.4). These are obtained by integrating the differential cross section (3.1) over the energy difference, given by ε, up to $\varepsilon_{\max}$, as well as over the polar angles, θ_j, for $0 \le |\cos\theta_j| \le \cos\theta_c$:

$$\frac{2\pi}{\sigma^{(h)}[\cos\theta_c]}\frac{\mathrm{d}\sigma^{(h)}[\cos\theta_c]}{\mathrm{d}\phi} = \frac{2\pi}{\sigma^{(h)}[\cos\theta_c]}\int_0^{\varepsilon_{\max}}\mathrm{d}\varepsilon\int_{-\cos\theta_c}^{\cos\theta_c}\mathrm{d}\cos\theta_1\int_{-\cos\theta_c}^{\cos\theta_c}\mathrm{d}\cos\theta_2 \times \frac{\mathrm{d}^4\sigma^{(h)}}{\mathrm{d}\varepsilon\,\mathrm{d}\cos\theta_1\,\mathrm{d}\cos\theta_2\,\mathrm{d}\phi}, \quad (5.1)$$

with

$$\sigma^{(h)}[\cos\theta_c] = \int_0^{\varepsilon_{\max}}\mathrm{d}\varepsilon\int_{-\cos\theta_c}^{\cos\theta_c}\mathrm{d}\cos\theta_1\int_{-\cos\theta_c}^{\cos\theta_c}\mathrm{d}\cos\theta_2 \times \int_0^{2\pi}\mathrm{d}\phi\,\frac{\mathrm{d}^4\sigma^{(h)}}{\mathrm{d}\varepsilon\,\mathrm{d}\cos\theta_1\,\mathrm{d}\cos\theta_2\,\mathrm{d}\phi}. \quad (5.2)$$

In this case, there is no particular need to use the events where the final-state electrons are close to the beam direction, so we impose a stronger cut, $\cos\theta_c = 0.9$. (It may even be difficult to determine the azimuthal angles for electrons which are close to the beam direction.) Results are shown in Figs. 7 ($m_h = 120$ GeV) and 8 ($m_h = 250$ GeV), for the unpolarized case, and for two c.m. energies. The distributions generally favor the region around $\phi \sim \pi$; i.e., the region where the two final-state electrons have non-vanishing and opposite transverse momenta (with respect to the beam), as opposed to $\phi \sim 0$, when they are more parallel. This broad feature is purely kinematic; more energy is available to create a Higgs particle if the two virtual Zs have opposite transverse momenta. In addition to this broad feature, there is a dip around $\phi = \pi$ in the CP-odd case, if the Higgs momentum is sufficiently high (i.e., at low mass).

If the two beams have opposite polarizations, the difference between the two cases can be quite spectacular, as is illustrated in Fig. 9 for $CP = 1$ and $CP = -1$.

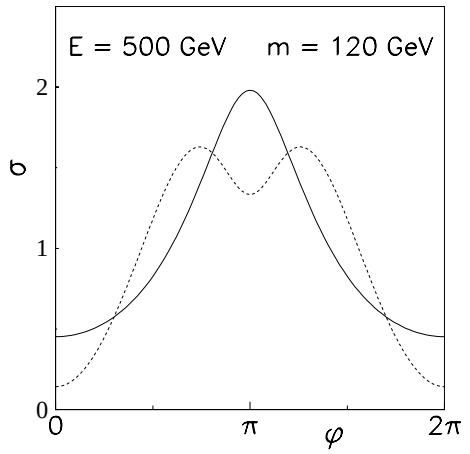

a

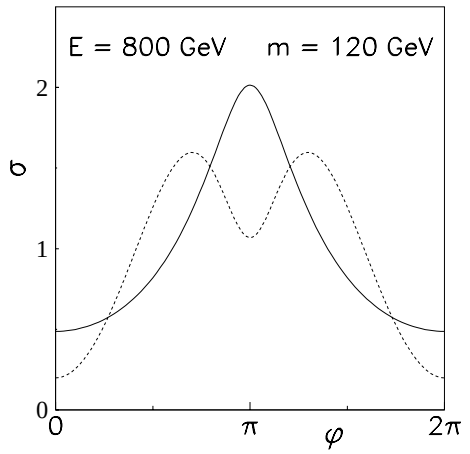

b

Fig. 7a,b. Azimuthal distributions at energies $E_{\mathrm{c.m.}} = 500$ GeV and 800 GeV, and for a Higgs mass $m_h = 120$ GeV, with unpolarized beams. Solid curves are for $CP = 1$, dashed ones are for $CP = -1$. The polar-angle cut-off is given by $\cos\theta_{\mathrm{c}} = 0.9$

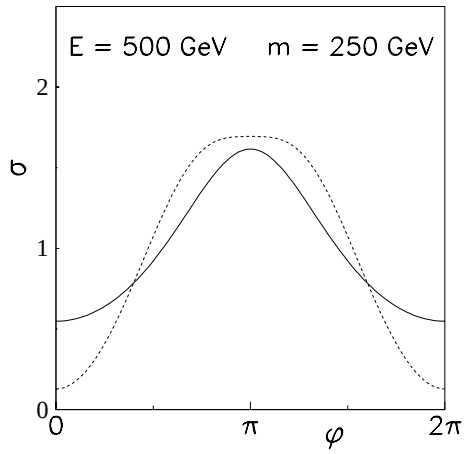

a

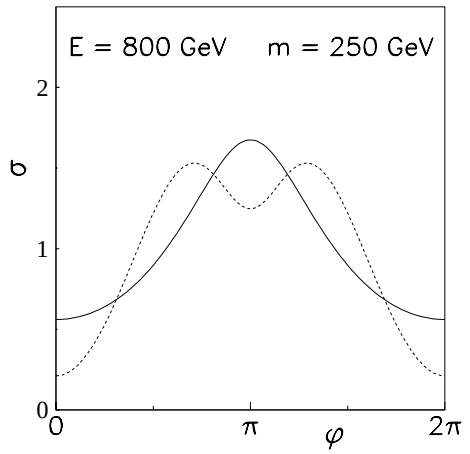

b

Fig. 8a,b. Same as Fig. 7 for $m_h = 250$ GeV

5.2 Polar-angle correlations

Next we consider distributions in the polar angles of the electrons:

$$\frac{1}{\sigma^{(h)}[\cos\theta_c]}\frac{\mathrm{d}^2\sigma^{(h)}}{\mathrm{d}\cos\theta_1\mathrm{d}\cos\theta_2} = \frac{1}{\sigma^{(h)}[\cos\theta_c]}\int_0^{\varepsilon_{\max}}\mathrm{d}\varepsilon \times\int_0^{2\pi}\mathrm{d}\phi\,\frac{\mathrm{d}^4\sigma^{(h)}}{\mathrm{d}\varepsilon\,\mathrm{d}\cos\theta_1\,\mathrm{d}\cos\theta_2\,\mathrm{d}\phi}. \quad (5.3)$$

Such a distribution is shown in Fig. 10 for $m_h = 120$. There is a rather strong difference between the two CP cases, the cross section being much more peaked for electrons emitted close to the forward direction in the CP-even case. To produce an odd parity state, angular momentum has to be transferred, and the electrons must therefore undergo a more violent scattering. For a higher Higgs mass, the effect is less pronounced.

A less-differential distribution can be obtained as follows. Let

$$\cos\Theta = \tfrac{1}{2}(\cos\theta_1 - \cos\theta_2), \quad (5.4)$$

or

$$\cos\theta_1 = \cos\Theta + \tfrac{1}{2}w, \qquad \cos\theta_2 = -\cos\Theta + \tfrac{1}{2}w, \quad (5.5)$$

and consider

$$\frac{1}{\sigma^{(h)}[\cos\theta_c]}\frac{\mathrm{d}\sigma^{(h)}}{\mathrm{d}\cos\Theta} = \frac{1}{\sigma^{(h)}[\cos\theta_c]}\int_0^{\varepsilon_{\max}}\mathrm{d}\varepsilon\int_0^{2\pi}\mathrm{d}\phi\int_{-w_{\max}}^{w_{\max}}\mathrm{d}w \times\frac{\mathrm{d}^4\sigma^{(h)}}{\mathrm{d}\varepsilon\,\mathrm{d}\cos\theta_1\,\mathrm{d}\cos\theta_2\,\mathrm{d}\phi} \quad (5.6)$$

with

$$w_{\max} = \begin{cases} 2(\cos\theta_c + \cos\Theta) & \text{if } \cos\Theta < 0, \\ 2(\cos\theta_c - \cos\Theta) & \text{if } \cos\Theta > 0. \end{cases} \quad (5.7)$$

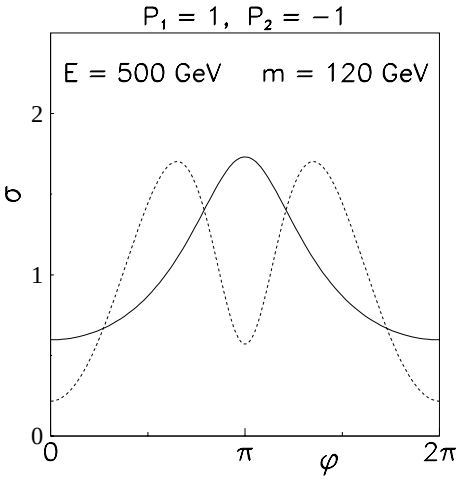

Fig. 9. Azimuthal distributions at $E_{\mathrm{c.m.}} = 500$ GeV, $m_h = 120$ GeV, for $P_1 = 1$ and $P_2 = -1$. The polar-angle cut-off is given by $\cos\theta_{\mathrm{c}} = 0.9$

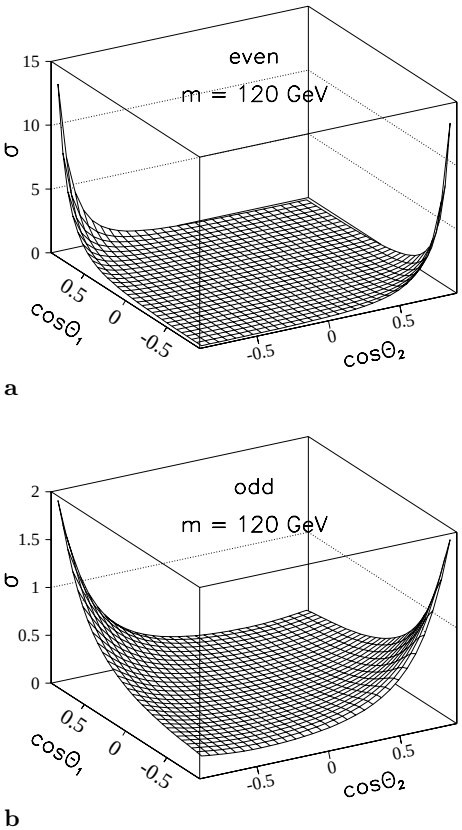

Fig. 10a,b. Normalized distributions, in the polar angles of the final-state electrons, $|\cos\theta_{1,2}| \leq 0.9$, for $E_{\mathrm{c.m.}} = 500$ GeV, $m_h = 120$ GeV, and for unpolarized beams. Note different scales

We show such distributions in Fig. 11, for the even and odd cases. For $CP = 1$, the cross section is much more peaked towards the forward direction, $\cos\Theta = \pm 1$, consistent with Fig. 10.

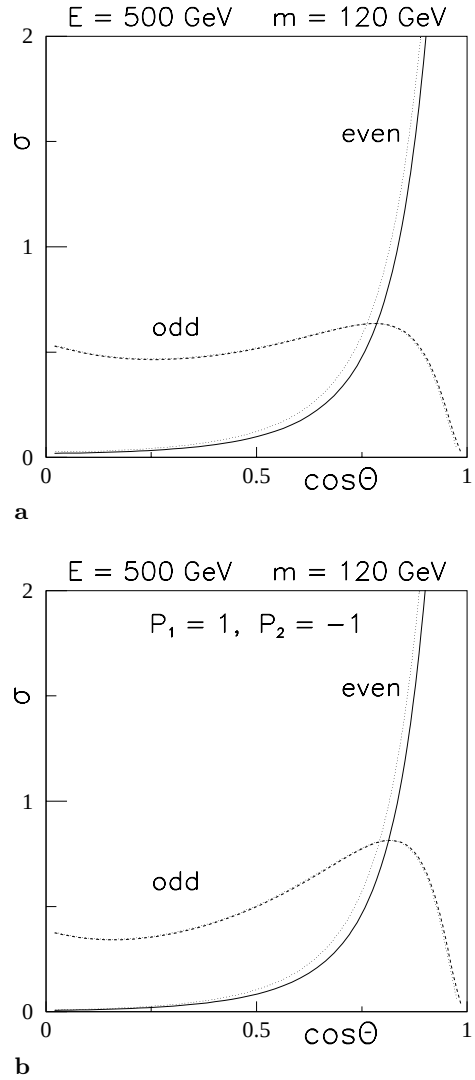

Fig. 11a,b. Distributions in $\cos\Theta$, for $E_{\mathrm{c.m.}} = 500$ GeV, $m_h = 120$ GeV, and **a** unpolarized beams, **b** $P_1 = 1$, $P_2 = -1$. Solid and dashed lines: cut at 5°; dotted lines: cut at 10°

5.3 Energy correlations

Finally, we consider the distribution in relative electron–energy difference. Introducing the scaled energy difference as $x = \varepsilon/\varepsilon_{\max}$ (see (3.5) and (3.6)), we will consider

$$\frac{1}{\sigma^{(h)}[\cos\theta_c]} \frac{\mathrm{d}\sigma^{(h)}[\cos\theta_c]}{\mathrm{d}x}. \tag{5.8}$$

Such distributions are shown in Fig. 12. For the CP-odd case, this distribution is "harder"; i.e., it falls off less rapidly for large energy differences x.

In electron–positron annihilation, with Higgs production via the Bjorken process, analogous distributions also exhibit a considerable sensitivity to whether the Higgs particle is even or odd under CP [11].

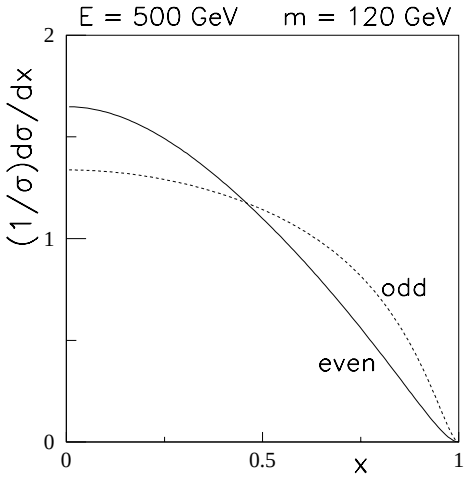

Fig. 12. Distributions in relative final-state electron energy, $x = \varepsilon/\varepsilon_{\max}$, for $E_{\rm c.m.} = 500$ GeV, $m_h = 120$ GeV, and unpolarized beams

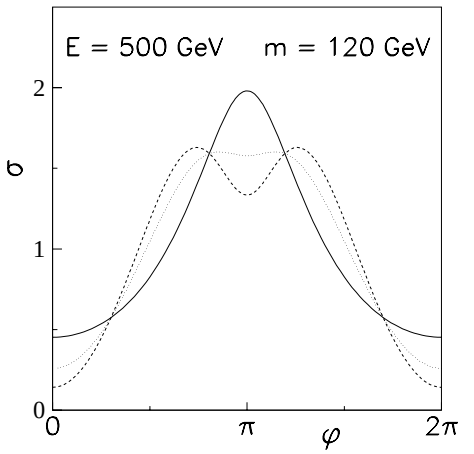

Fig. 13. Azimuthal distributions for $E_{\rm c.m.} = 500$ GeV, $m_h = 120$ GeV. Solid: $CP = +1$, dashed: $CP = -1$, dotted: CP violated, with $\eta = 0.5$. Polar-angle cuts: $|\cos\theta_c| \le 0.9$

6 CP violation

As discussed in the introduction, there could also be CP violation in the Higgs sector, in which case the Higgs particles would not be eigenstates of CP.

While the presence of both even ($X^{(H)}$ and $Z^{(H)}$) and odd ($X^{(A)}$ and $Z^{(A)}$) terms in the cross section reflect parity violation, only the terms $\tilde{X}_t$ and $\tilde{X}_u$ explicitly violate parity. For these to be observed, one has to assign a value to $\boldsymbol{p}_1' \times \boldsymbol{p}_2'$ (cf. (3.19)), i.e., one needs to distinguish the final-state electrons.

We show in Fig. 13 azimuthal distributions of the kind shown in Figs. 7 and 8, allowing for CP violation. Since these involve a symmetrical integration over both hemispheres, $-\cos\theta_c \le \cos\theta_{1,2} \le \cos\theta_c$, the parity-violating terms $\tilde{X}_t$ and $\tilde{X}_u$ (cf. (3.20)) are cancelled. However, the parity violation leads to a superposition of the two cases, $CP = +1$ and $CP = -1$. Such distributions may suffice to provide evidence of parity violation.

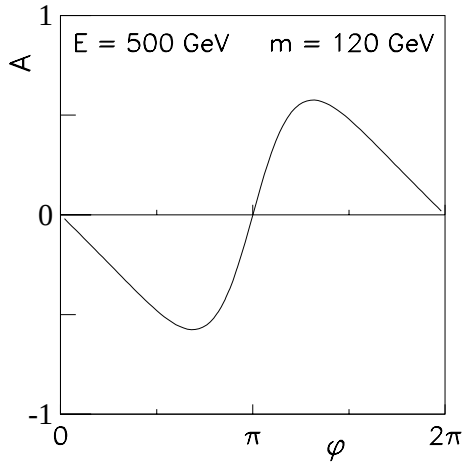

Fig. 14. CP-violating asymmetry A of (6.1), for $E_{\rm c.m.} = 500$ GeV, $m_h = 120$ GeV, and $\eta = 0.5$. Polar-angle cuts: $|\cos\theta_c| \le 0.9$

One way to access the parity-violating terms $\tilde{X}_t$ and $\tilde{X}_u$ is to introduce the weight factor $\cos\theta_1$ to distinguish the two hemispheres. Thus, we consider (the two electrons are here distinguished by $E_1' > E_2'$) the asymmetry

$$A = \frac{2\pi}{\sigma^{(h)}[\cos\theta_c]} \int_0^{\varepsilon_{\max}} \mathrm{d}\varepsilon \int_{-\cos\theta_c}^{\cos\theta_c} \mathrm{d}\cos\theta_1 \times \int_{-\cos\theta_c}^{\cos\theta_c} \mathrm{d}\cos\theta_2 \frac{\mathrm{d}^4\sigma^{(h)}\ \cos\theta_1}{\mathrm{d}\varepsilon\,\mathrm{d}\cos\theta_1\,\mathrm{d}\cos\theta_2\,\mathrm{d}\phi}. \quad (6.1)$$

This quantity is shown in Fig. 14 for the same parameters and cuts as those used in Fig. 13. To lowest order, the effect is linear in η. Thus, given enough data, the effect can be sizable. Other ways to search for CP violation in the ZZ–Higgs coupling are discussed in [10,11,14].

7 Charged Higgs production

If the produced Higgs is charged, there will be one or two final-state neutrinos. These cannot be detected, so distributions of the kind discussed in Sect. 5 are not available. One may instead consider distributions of the charged Higgs particles themselves.

7.1 Singly-charged Higgs production

Singly-charged (negative) Higgs particles, which are expected in certain models [15], can be produced in e^-e^- collisions through the exchange of one Z and one W^- boson. The cross section would be given by formulas analogous to those presented in Sect. 3, where the numerical coefficients involving the polarizations P_i and the relative strength of the axial coupling, $\sin 2\chi$, would be replaced as follows for the t-channel terms (with accompanying changes in the

propagator masses):

$$(1 - P_1 \sin 2\chi)(1 - P_2 \sin 2\chi) \to (1 - P_1 \sin 2\chi)(1 - P_2),$$
$$(\sin 2\chi - P_1)(\sin 2\chi - P_2) \to (\sin 2\chi - P_1)(1 - P_2), \tag{7.1}$$

and similarly for the u-channel terms, with P_1 and P_2 interchanged. The interference terms would have the coefficient substitution

$$(1 + P_1P_2)(1 + \sin^2 2\chi) - 2(P_1 + P_2)\sin 2\chi$$
$$\to (1 - P_1)(1 - P_2)(1 + \sin 2\chi), \tag{7.2}$$

where $\sin 2\chi \simeq 0.1393$ refers to the eeZ coupling.

These substitutions would change only quantitative aspects of the cross sections. Thus, we expect all qualitative features discussed in Sect. 4 to remain valid.

7.2 Doubly-charged Higgs production

Doubly-charged Higgs particles, h^{--}, which are expected in the left–right-symmetric [9] and other models [8], can be produced in electron–electron collisions, not only in the s-channel, but also via WW exchange. This mechanism does not require lepton-number violation, but the WWh^{--} coupling is absent in certain models [5]. Apart from an overall, model-dependent constant, the cross section would be given by the formulas of Sect. 3, with $\sin 2\chi = 1$. Distributions of the kinds given in Figs. 4 and 6 would readily reveal whether such a particle was even or odd under CP.

8 Statistical considerations

It is of interest to estimate how many events are needed to determine the CP from distributions of the kinds presented here. One of the most promising ones appears to be the Higgs energy distribution, shown in Fig. 4. We will assume that CP is conserved, so that the problem can be formulated in terms of statistical hypothesis testing as H_0: $CP = 1$ and H_1: $CP = -1$. Information would be gained if H_0 were rejected.

We denote the $CP = +1$ distribution by $f(x)$ and the $CP = -1$ distribution by $g(x)$. The problem is well suited for the Neyman–Pearson test [21], and following this approach, we will reject H_0 if, for n events, the likelihood ratio

$$L(x_1, x_2, \ldots, x_n) = \frac{g(x_1)g(x_2)\cdots g(x_n)}{f(x_1)f(x_2)\cdots f(x_n)} \geq k, \tag{8.1}$$

where x_i denote observed values of E_h, and
k is a critical constant to be determined.
The constant k determines α, the level of "significance" of the test, i.e., the probability that we reject a *correct* hypothesis. An estimate for k can be obtained by Monte Carlo simulations. By drawing s samples of n x-values from the $f(x)$ distribution, the ratios $L_1, L_2, \ldots L_s$ can be calculated by applying (8.1). The empirical $(1-\alpha)\times 100\%$ percentile in the simulated L distribution can be used as an estimate of k.

Table 1. Recognition probabilities. Here, n is the number of events, the level of significance of the test is $\alpha = 5\%$, and $1-\beta$ [%] is the probability that one can recognize a $CP = -1$ distribution in Higgs energy data, for $E_{\text{c.m.}} = 500$ GeV and at three Higgs masses, $m_h = 100$, 120 and 150 GeV. See the text for further details

		100 GeV		120 GeV		150 GeV	
	n	k	1-β	k	1-β	k	1-β
No cut	5	3.0	81	3.2	80	3.5	76
	10	0.75	97	0.94	97	1.2	95
Cut at 10°	5	3.2	80	3.4	76	3.6	72
	10	1.0	96	1.2	95	1.5	93

The "power" of this test, $1 - \beta$ (the probability of rejecting H_0 when H_0 is false), can also be estimated by Monte Carlo simulations. Samples should then be drawn from the g distribution, and the proportion of samples that are rejected in the test estimates $1 - \beta$. Results are given in Table 1 for $E_{\text{c.m.}} = 500$ GeV and three values of the Higgs mass, $m_h = 100$, 120 and 150 GeV. For each mass value, two cases are considered: (i) no cut on the final-state electron momenta, (ii) the electron momenta have to satisfy $\theta \geq 10°$. (With a cut at 5°, these probabilities are practically the same as without any cut.) At a mass of 120 GeV, we see that 10 events suffice to reveal a $CP = -1$ distribution, at the level of 95–97%, with a risk of falsely rejecting the correct hypothesis, α, of only 5%. The discrimination is easier if one can get data near the beam direction, and if the Higgs particle is light, as is also seen from Fig. 4.

9 Concluding remarks

We have studied the production of generic Higgs particles in e^-e^- collisions, focusing on distributions which might be useful in distinguishing a CP-even from a CP-odd particle. Longitudinal beam polarization effects are taken into account. We have not discussed backgrounds. These would depend on how the Higgs boson is detected. A light Higgs would dominantly decay to b quarks, and the background would not be severe, occurring mainly from single Z and W production and the two-photon process [6]. A heavier Higgs would decay to W and Z bosons, and the background would be a problem [3,22]. In the CP-even case, the Higgs particle tends to be softer, and events are more aligned with the beam direction than in the CP-odd case. In fact, the Higgs energy distribution may be one of the better observables for discriminating the two cases. Furthermore, the dependence on the *product* of the two beam polarizations is much larger in the CP-odd case. This dependence, which is represented by an observable A_1, becomes a better "discriminator" for increasing Higgs masses when the Higgs momentum decreases, and other methods may tend to become less efficient.

If the two final-state electrons are observed, a certain azimuthal distribution, as well as the electron polar-angle distributions, will also be useful for discriminating the two cases.

Finally, we suggest ways to search for possible parity-violating effects in the ZZ–Higgs coupling.

Acknowledgements. It is a pleasure to thank C. Irgens, P. Minkowski, C. Newton and T. T. Wu for most valuable discussions. This research has been supported by the Research Council of Norway. JZZ would like to thank those in the Department of Physics, University of Bergen, for their warm hospitality. His work has been supported by the National Natural Science Foundation of China under Grant No. 19674014, and by the Shanghai Education Development Foundation.

Appendix A. The e^+e^- cross section

For the positron–electron case, there is, in addition to the familiar Bjorken diagram, also a t-channel diagram. The cross section can be expressed as

$$\frac{\mathrm{d}^4\sigma^{(h)}}{\mathrm{d}\varepsilon\,\mathrm{d}\cos\theta_1\,\mathrm{d}\cos\theta_2\,\mathrm{d}\phi} = C^{(h)}\big\{[F(t_1,t_2)]^2\,X^{(h)} + [F(s_1,s_2)]^2\,\tilde{X}^{(h)} + 2\mathrm{Re}[F^*(s_1,s_2)F(t_1,t_2)]Z^{(h)}\big\}, \tag{A.1}$$

with $F(t_1,t_2)$ defined by (3.2). The amplitude for the t-channel diagram is related to the corresponding one for the electron–electron case by the spinor substitutions $\bar{v}(p_1)\to\bar{u}(p_1')$, and $v(p_1')\to u(p_1)$, which amount to $(s_1,s_2)\leftrightarrow(-u_2,-u_1)$. Also, the convention for the positron polarization is different, such that $P_1\to -P_1$.

Furthermore, the (s-channel) Bjorken diagram is related to the t-channel diagram in a way similar to what is the case for the electron–electron diagrams. Thus, the unpolarized cross section for the Bjorken diagram is related to that of the t-channel diagram by $(s_1,s_2)\leftrightarrow(-t_1,-t_2)$. However, the positron polarization for the Bjorken diagram would correspond to a final-state polarization in the t-channel diagram (which we sum over). Thus, the polarization-dependent parts of these cross sections are not related in this simple way.

For the CP-even case, we find

$$\begin{aligned} X^{(H)} &= 2\big[(1+P_1\sin 2\chi)(1-P_2\sin 2\chi)(s_1s_2+u_1u_2) \\ &\quad -(\sin 2\chi+P_1)(\sin 2\chi-P_2)(s_1s_2-u_1u_2)\big] \\ &= 2[(1+P_1P_2)(1-\sin^2 2\chi)s_1s_2 \\ &\quad +(1-P_1P_2)(1+\sin^2 2\chi)u_1u_2 \\ &\quad +2(P_1-P_2)\sin 2\chi u_1u_2], \end{aligned} \tag{A.2}$$

$$\tilde{X}^{(H)} = 2\{(1-P_1P_2)[t_1t_2+u_1u_2-\sin^2 2\chi(t_1t_2-u_1u_2)] + 2(P_1-P_2)\sin 2\chi u_1u_2\}, \tag{A.3}$$

$$Z^{(H)} = 2[(1-P_1P_2)(1+\sin^2 2\chi)+2(P_1-P_2)\sin 2\chi] \times u_1u_2. \tag{A.4}$$

For the CP-odd case, we find

$$\begin{aligned} X^{(A)} &= \frac{t_1t_2}{2}\big[(s_1+s_2)^2+(u_1+u_2)^2\big]-(s_1s_2-u_1u_2)^2 \\ &\quad -(t_1t_2)^2-\sin^2 2\chi\,\frac{t_1t_2}{2}\big[(s_1-s_2)^2-(u_1-u_2)^2\big] \\ &\quad +(P_1-P_2)\sin 2\chi\Big[t_1t_2(u_1^2+u_2^2)-(s_1s_2)^2 \\ &\quad -(t_1t_2)^2-(u_1u_2)^2+2s_1s_2(t_1t_2+u_1u_2)\Big] \\ &\quad +P_1P_2\bigg\{\frac{t_1t_2}{2}[(s_1-s_2)^2-(u_1-u_2)^2] \\ &\quad +\sin^2 2\chi\bigg(-\frac{t_1t_2}{2}\big[(s_1+s_2)^2+(u_1+u_2)^2\big] \\ &\quad +(s_1s_2-u_1u_2)^2+(t_1t_2)^2\bigg)\bigg\}, \end{aligned} \tag{A.5}$$

$$\begin{aligned} \tilde{X}^{(A)} &= \frac{s_1s_2}{2}\big[(t_1+t_2)^2+(u_1+u_2)^2\big]-(t_1t_2-u_1u_2)^2 \\ &\quad -(s_1s_2)^2-\sin^2 2\chi\frac{s_1s_2}{2}[(t_1-t_2)^2-(u_1-u_2)^2] \\ &\quad +(P_1-P_2)\sin 2\chi\Big[s_1s_2(u_1^2+u_2^2)-(s_1s_2)^2 \\ &\quad -(t_1t_2)^2-(u_1u_2)^2+2t_1t_2(s_1s_2+u_1u_2)\Big] \\ &\quad +P_1P_2\bigg\{-\frac{s_1s_2}{2}[(t_1+t_2)^2+(u_1+u_2)^2] \\ &\quad +(t_1t_2-u_1u_2)^2+(s_1s_2)^2 \\ &\quad +\sin^2 2\chi\frac{s_1s_2}{2}[(t_1-t_2)^2-(u_1-u_2)^2]\bigg\}, \end{aligned} \tag{A.6}$$

$$\begin{aligned} Z^{(A)} &= \frac{1}{4}\big[(1-P_1P_2)(1+\sin^2 2\chi)+2(P_1-P_2)\sin 2\chi\big] \\ &\quad \times\big[2(s_1s_2-t_1t_2)^2+u_1u_2(u_1^2+u_2^2) \\ &\quad -(s_1s_2+t_1t_2)(u_1+u_2)^2\big]. \end{aligned} \tag{A.7}$$

References

1. M. Tigner, B. Wiik, F. Willeke, Particle Accel. Conf. IEEE, 2910 (1991); S. Kuhlman et al. (The NLC ZDR Design Group and the NLC Physics Working Groups), "Physics and Technology of the Next Linear Collider: A Report Submitted to Snowmass '96", BNL 52-502, FERMILAB-PUB-96/112, LBNL-PUB-5425, SLAC-Report-485, UCRL-ID-124160, UC-414 (June 1996); H. Murayama, M. E. Peskin, Ann. Rev. Nucl. Part. Sci. **46**, 533 (1996); "e+e− Linear Colliders: Physics and Detector Studies", R. Settles, editor, Proceedings and workshops, ECFA/DESY, Frascati, London, Munich, Hamburg, DESY-97-123E, 1997
2. E. Accomando et al., Phys. Rep. **299**, 1 (1998)
3. K. I. Hikasa, Phys. Lett. B **164**, 385 (1985), Err. ibid. B **195**, 623 (1987)
4. See, for example: C. A. Heusch, SCIPP-95-02, 1995, Talk given at 1st Arctic Workshop on Future Physics and Accelerators, Saariselka, Finland, August 1994, Published in Arctic Physics Workshop 1994; F. Cuypers, Talk given

at 3rd Workshop on Physics and Experiments with e+ e− Linear Colliders, (LCWS95), Iwate, Japan, MPI-PHT-95-127 (hep-ph/9512201); F. Cuypers, Int. J. Mod. Phys. A **11**, 1571 (1996) ; T. G. Rizzo, Int. J. Mod. Phys. A **11**, 1613 (1996); B. Ananthanarayan, P. Minkowski, Phys. Lett. B **373**, 130 (1996); F. Cuypers, M. Raidal, Nucl. Phys. B **501**, 3 (1997); H. E. Haber, Int. J. Mod. Phys. A **13**, 2263 (1998)

5. J. F. Gunion, Int. J. Mod. Phys. A **11**, 1551 (1996)
6. V. Barger, J. F. Beacom, Kingman Cheung, T. Han, Phys. Rev. D **50**, 6704 (1994); T. Han, Int. J. Mod. Phys. A **11**, 1541 (1996); P. Minkowski, Int. J. Mod. Phys. A **13**, 2255 (1998)
7. J. D. Bjorken, in Proceedings of the 1976 SLAC Summer Institute on Particle Physics, ed. M. Zipf (SLAC Report No. 198, 1976) p. 22; B.L. Ioffe, V.A. Khoze, Sov. J. Part. Nucl. **9**, 50 (1978); D.R.T. Jones, S.T. Petcov, Phys. Lett. **84B**, 440 (1979); J. Finjord, Physica Scripta **21**, 143 (1980)
8. H. Georgi, M. Machacek, Nucl. Phys. B **262**, 463 (1985); R. Vega, D. A. Dicus, Nucl. Phys. B **329**, 533 (1990); J. F. Gunion, R. Vega, J. Wudka, Phys. Rev. D **42**, 1673 (1990)
9. J. C. Pati, A. Salam, Phys. Rev. D **10**, 275 (1974); R. N. Mohapatra, J. C. Pati, Phys. Rev. D **11**, 566 (1975); G. Senjanovic, R. N. Mohapatra, Phys. Rev. D **12**, 1502 (1975); R. E. Marshak, R. N. Mohapatra, Phys. Lett. **91B**, 222 (1980)
10. D. Chang, W. Y. Keung, I. Phillips, Phys. Rev. D **48**, 3225 (1993); A. Skjold, P. Osland, Phys. Lett. B **311**, 261 (1993); B **329**, 305 (1994); B. A. Kniehl, *Proc. Workshop on Physics and Experiments with Linear e^+e^- Colliders*, Waikoloa, Hawaii, April 26–30, 1993 vol. II, p. 625; V. Barger, K. Cheung, A. Djouadi, B. A. Kniehl, P. M. Zerwas, Phys. Rev. D **49**, 79 (1994); K. Hagiwara, M. L. Stong, Z. Phys. C **62**, 99 (1994); M. L. Stong, Invited talk, Ringberg Workshop *Perspectives for Electroweak Interactions in e^+e^- Collisions*, Munich, Feb. 5–8, 1995, hep-ph/9504345
11. A. Skjold, P. Osland, Nucl. Phys. B **453**, 3 (1995)
12. T. Arens, U. D. J. Gieseler, L. M. Sehgal, Phys. Lett. B **339**, 127 (1994); T. Arens, L. M. Sehgal, Z. Phys. C **66**, 89 (1995)
13. O. M. Ogreid, in *XI International Workshop: High Energy Physics and Quantum Field Theory*, Proceedings of the conference, St. Petersburg, Russia, ed. B.B. Levtchenko, Moscow University Press (Moscow, 1997) 189, hep-ph/9701245
14. J. R. Dell'Aquila, C. A. Nelson, Phys. Rev. D **33**, 101 (1986); D. Chang, W.-Y. Keung, I. Phillips, Phys. Rev. D **48**, 3225 (1993)
15. J. F. Gunion, H. E. Haber, G. Kane, S. Dawson, *The Higgs Hunter's Guide*, Addison-Wesley, New York, 1990
16. For a recent review, see, W. Bernreuther, Lectures given at 37th Internationale Universitätswochen für Kernphysik und Teilchenphysik, Schladming, Austria, 28 Feb–7 Mar 1998; hep-ph/9808453
17. N. G. Deshpande, E. Ma, Phys. Rev. D **16**, 1583 (1977); M. Matsuda, M. Tanimoto, Phys. Rev. D **52**, 3100 (1995)
18. A. Pilaftsis, Phys. Rev. Lett. **77**, 4996 (1996); Nucl. Phys. B **504**, 61 (1997); Phys. Lett. B **435**, 88 (1998)
19. G. Altarelli, R. Barbieri, F. Caravaglios, Int. J. Mod. Phys. A **13**, 1031 (1998)
20. H. A. Olsen, P. Osland, Phys. Rev. D **25**, 2895 (1982)
21. W. T. Eadie, et al., *Statistical methods in experimental physics*, North-Holland, 1971, Chapter 10
22. F. Cuypers, R. Kołodziej, O. Korakianitis, R. Rückl, Phys. Lett. B **325**, 243 (1994); F. Cuypers, R. Kołodziej, R. Rückl, Nucl. Phys. B **430**, 231 (1994)